Temporal trajectories of human brown and white adipocyte progenitors at single cell resolution

Nagendra Palani
The Novo Nordisk Foundation Center for Basic Metabolic Research
Pascal Timshel
The Novo Nordisk Foundation Center for Basic Metabolic Research
Pytrik Folkertsma
The Novo Nordisk Foundation Center for Basic Metabolic Research
Alexander Grønning
The Novo Nordisk Foundation Center for Basic Metabolic Research
Tora Henriksen
Centre for Physical Activity Research
Lone Peijs
The Novo Nordisk Foundation Center for Basic Metabolic Research
Verena Jensen
Steno Diabetes Center Copenhagen
Karolina Hvid
Centre for Physical Activity Research
Wenfei Sun
Laboratory of Translational Nutrition Biology, ETH Zurich
Naja Jespersen
Rigshospitalet https://orcid.org/0000-0002-3488-1657
Christian Wolfrum
ETH Zürich https://orcid.org/0000-0002-3862-6805
Tune Pers
University of Copenhagen https://orcid.org/0000-0003-0207-4831
Søren Nielsen
University Hospital of Copenhagen https://orcid.org/0000-0002-3119-750X
Camilla Scheele (✉ cs@sund.ku.dk)
The Novo Nordisk Foundation Center for Basic Metabolic Research https://orcid.org/0000-0002-6055-9709

Article

Keywords:

Posted Date: February 10th, 2022

DOI: https://doi.org/10.21203/rs.3.rs-1328581/v1

Version of Record: A version of this preprint was published at Nature Metabolism on June 19th, 2023. See the published version at https://doi.org/10.1038/s42255-023-00820-z.

Abstract

Adipose tissue type and distribution are major determinants of metabolic disease, warranting investigations of depot-defining mechanisms. Here we show that progenitor cells from four human brown and white adipose depots separate into two main cell fates, a metabolic and a structural branch, during early differentiation at single cell resolution. The metabolic cell type expresses Adiponectin and is driven by an adipogenic transcriptional network including *PPARG.* Halfway through maturation, these cells have a brown adipocyte signature regardless of adipose depot origin. The structural cell type arises from the same progenitors as the metabolic cell type but expresses extracellular matrix factors and is driven by a competing osteoblast transcription factor network. The metabolic adipocyte gene signature associates with traits for fat distribution. In conclusion, we provide a seamless differentiation map of human adipocytes, providing an insight in the WAT browning process and a long-term perspective of cell-type specific targeting of metabolic disease.

Introduction

Body fat distribution and quality are determinants of metabolic health. Multiple studies have revealed that abdominal obesity is strongly associated with cardiovascular disease and insulin resistance, whereas accumulation of fat in the lower gynoid regions has a lower lipid turnover and is associated with metabolic health[1]. In contrast to the common societal view that all excessive fat tissue is unhealthy, a functional adipose tissue allows for safe storage of excess calories. The essential role of safe lipid storage in a healthy adipose tissue is underscored by conditions like lipodystrophy, which is characterized by atypical accumulation of lipids and development of insulin resistance[2]. Adipocytes are lipid-storing and energy-transforming cells. Subtypes of adipocytes are linked to anatomical depots, displaying niche-defined functions. For example, the subcutaneous depot hosts white adipocytes with tremendous capacity for plasticity, in terms of energy access dependent lipogenesis and lipolysis plasticity[3]. In contrast, the supraclavicular deep neck depot contains brown adipocytes, which are heat producing with specialized uncoupling mitochondria that are turned on in response to cold induced sympathetic signals[4]. Adipocytes originate from mesenchymal stem cells that reside in multiple tissues including adipose tissue, skeletal muscle, and bone marrow[5]. Interestingly, studies suggest that brown adipocytes share some developmental similarities with the mitochondria-rich skeletal muscle cells[6]. Other studies have shown a close relation between osteocytes and adipocytes, which were found to share a transcriptional network[7]. It was found that this common network must be suppressed for cells to differentiate into adipocytes instead of osteocytes[7]. Intriguingly, it has been reported that progenitor cells derived from white adipose tissue of the brown bear, which exhibit an enormous seasonal plasticity, spontaneously differentiated into osteocytes in vitro[8], further emphasizing the developmental link between these two cell types.

Recent single cell technologies have allowed for understanding the heterogeneity of adipocytes at a higher resolution, revealing several subtypes with specialized functions[9–11]. These studies suggest that separate cell types provide thermogenesis, insulin sensitivity, lipid storage, and adipokine secretion[12,13] or act as negative regulators of lipid accumulation[14]. However, the developmental hierarchical heterogeneity of human brown and white adipogenic events remains elusive. Importantly, although tightly controlled in healthy conditions[15], there is a capacity for browning of WAT during extreme conditions of increased sympathetic activation, for example in patients suffering from pheochromocytoma[16,17] or burn injuries[18]. In the current study, we compared differentiating human adipocytes derived from two WAT depots; subcutaneous and visceral, and from two BAT depots; supraclavicular and perirenal. We used single-cell RNA sequencing (scRNA-seq) and performed temporal modeling of the transcriptional data to track transcriptional branching of cellular subtypes during adipogenesis of our multidepot-derived progenitor cells. We visualized the identified cellular subtypes with fluorescence in situ hybridization (FISH) imaging, using single cell targeting RNAscope probes. We further validated our *in vitro* findings in an *in vivo* single nucleus RNA sequencing (snRNA-seq) dataset of human BAT, and used the computational tool CELLECT to link cell specific gene signature with genetic variants in genome-wide association study (GWAS) data.

Results

Human WAT- and BAT-derived progenitors share cell fates during early differentiation

To investigate adipose depot differences, we cultured 14 different adipose progenitor cell strains derived from supraclavicular or perirenal BAT or from visceral or subcutaneous WAT of adult humans [19,20] (**Figure 1a**). We generated droplet-scRNA-seq data from these adipose progenitor cell strains. We used the R package Seurat for pre-processing the data, quality control, regression of cell cycle effects, sample alignment and differential expression analyses. We obtained 56,371 high-quality cells after quality control. For this initial analysis, cells were harvested at a proliferating, sub-confluent state ("**T1**") (**Figure 1a**). For each depot, we included cells from at least three different individuals, matched for age, sex and body mass index (BMI) (**Table S1**). However, cell cycle effects explained most of the variation in the data (**Figure S1**). We therefore regressed out cell cycle effects and kept both datasets for further analysis. We performed principal component analysis (PCA) and the first 12 principal components were used for t-SNE visualization of the data without cell cycle effects. The t-SNE visualization of the data without cell cycle effects regressed out shows that cells tend to group to their own sample and to the phase of the cell cycle they are in (**Figure S1**). To overcome possible batch effects, we aligned our samples with each other using canonical correlation analysis and dynamic time warping. A t-SNE visualization of the aligned data shows all samples aligned in one big cluster without any visible structure (**Figure S2**). The alignment almost completely captures cell cycle effects (**Figure S2**). A t-SNE visualization of the aligned data without cell cycle effects shows that the structure of the alignment does not change much when regressing out cell cycle effects (**Figure S2**). These analyses suggest that the unsupervised clustering of multidepot-derived adipocyte progenitors was based on sample-specific signals and cell cycle effects. In conclusion, our data suggest that undifferentiated, proliferating adipocyte progenitors have similar

expression patterns regardless of BAT or WAT origin (**Figure 1b**). The high degree of similarity between human brown and white adipocytes at this developmental stage was surprising given our previous findings that these cell-types are functionally different when fully differentiated[19,20]. However, despite lack of depot-dependent clustering, we decided to explore whether depot-dependent differences in single gene expression occurred. We thus performed differential expression (DE) analysis between the depots. We first performed DE tests for each depot against the contrary two depots. We found 181 genes for supraclavicular, 129 for perirenal, 116 for subcutaneous and 108 for visceral (Bonferroni corrected $P < 0.05$, absolute average log fold change > 0.25). However, after inspecting these genes, we observed that most genes were found because of sample-specific signals. Therefore, we also performed DE tests for each sample against the contrary two depots and only kept the intersecting genes for all samples belonging to the same depot. This resulted in a smaller list of differentially expressed genes per depot: 6 genes for supraclavicular, 19 for perirenal, 11 for subcutaneous and 26 for visceral (Bonferroni corrected $P < 0.05$, absolute average log fold change > 0.25) (**Table S12**). Because we used a low threshold for average log fold change, not all genes were equally important. For the brown adipocyte progenitor samples, 3 genes stood out. The first gene, *TM4SF1*, was higher expressed in both the perirenal and supraclavicular depots (average log FC 0.87 and 0.34 respectively) and was found for all perirenal samples and 2 of the supraclavicular samples (**Figure S3**). *LY6K* was also higher expressed in the perirenal and supraclavicular samples (average log FC of 0.33 and 0.38 respectively) and was found for 2 perirenal samples and 2 supraclavicular samples (**Figure S3**). Last, *HOXB7* was found as a negative marker gene for all supraclavicular samples (average log FC -0.42, **Figure S3**). Furthermore, we found two genes that seemed to discriminate the visceral samples well. *BARX1* was found to be higher expressed in a small part of the cells in the visceral samples (average log FC 0.25, **Figure S3**), and *LINC01116* was found as a negative gene for all visceral samples (average log FC -0.32, **Figure S3**). We next explored the data using Monocle and Velocyto, which underscored the similarities between the adipogenic progenitor cells, assigning cell cycle effects as the major driver of differences (**Figure S4**). We observed one small 'common cluster', distinct from the main cluster and with cells from all depots (**Figure 1b**). This cluster was negative for *CD29*, a surface marker previously proposed to be a predictive marker for adipogenic precursor cells with thermogenic potential[21]. This observation was intriguing as the main cluster consisted of adipocyte progenitors from all four BAT and WAT depots. We further characterized the two clusters by using scmap[22] to map our data set onto an existing catalogue of cell-types in murine tissues[23].

In this analysis, the main, CD29-positive cluster was enriched for adipogenic precursor markers, whereas the CD29-negative cluster was enriched for epithelial cell markers (**Figure S5**). Most genes distinguishing between brown and white adipocytes, including UCP1, are not expressed until later in differentiation[24]. Thus, to discover transcriptional branching avenues between adipocyte progenitors derived from supraclavicular, perirenal, subcutaneous and visceral adipose depots, we harvested cells from all four depots during four additional time points **T2-T5** during differentiation (**Figure 1a**, **Table S1**) and performed single-cell transcriptomics, obtaining 23,428 high-quality cells (**Figure S6**). At T3, cells were two days post-confluence and a differentiation initiation cocktail was added (please see methods for

components). Cells were subsequently harvested at T4 and T5, representing three and six days following addition of the differentiation cocktail, respectively. It should be noted that the full differentiation protocol into mature adipocytes is 12 days from the addition of the differentiation media[25]. However, changes in cell morphology are initiated shortly after adding the cell differentiation media and at T5 (corresponding to 6 days after adding the differentiation media), some accumulation of small lipid droplets has started. The analysis resulted in clearly separated cell clusters both by time point and by depot within T4 and T5, whereas a PCA plot of the data shows that cell identities from T1-T3 are overlapping (**Figure 1c, Figure S6**). To assess common or distinct developmental trajectories across depots, we used Monocle[26] to order cells in 'pseudotime' - a quantitative measure of progress through a biological process (**Figure 1d**). Notably, we applied a data-driven approach that did not include prior information on adipose depot origin of the cells. The trajectory topology was robust to changes in the input and parameter settings of the Monocle trajectory algorithm (**Figure S7**). The trajectory analysis revealed bifurcating cell fates of adipose progenitor cells from the four different depots of human BAT and WAT. Cells from T1-T3 formed a progenitor (P) branch. In line with our initial analysis of proliferating precursor cells, cells from the earlier time points (T1-T3) did not separate in pseudotime and cells from all depots contributed equally to the (P) branch (**Figure 1d**). Later in pseudotime, cells separated into two branches: upper branch (U branch) and lower branch (L branch) containing cells after induction of differentiation (T4 and T5) (**Figure 1d**). Following branching, we observed a depot-dependent asymmetry in cell distribution where the U branch was dominated by cells from the brown fat depots (>60%) while cells from the white fat depots (>60%) were overrepresented in the L branch. Importantly, all four depots contributed to both upper and lower cell branches, suggesting a striking similarity also at this later developmental stage, (**Figure 1d**). When t-SNE plots of cell branch identity was overlaid with time point and depot label, the branch separation occurring at both T4 and T5 was clear (**Figure 1e**). Interestingly, a subpopulation of cells at T5, dominated by cells derived from the supraclavicular depot but including cells from all depots, was assigned to the P branch (**Table S3**). These cells were only sporadically expressed at T4 and clustered in the late part of the P branch in pseudotime, suggesting that dedifferentiation had occurred (**Figure S7**). The mechanism of dedifferentiation of adipocytes has been previously reported[27] and might reflect the ability of adipocytes to interconvert[28]. Supporting that dedifferentiation had occurred, DE genes between the T5 P branch cells and the T1-T3 P branch cells revealed residual high expression of both U branch and L branch specific markers, suggesting unbiased contribution of dedifferentiated cells and gradual loss of branch specific markers. These findings also emphasize that neither of the cells in the U branch or L branch were undifferentiated or dedifferentiated progenitor cells, but rather represented two separate cell fates present among differentiating adipocytes. Importantly, we were able to confirm the differentiation trajectories predicted by Monocle pseudotime using an independent method called Velocyto[29] (**Figure S8**).

The identified cell fates are also present in human BAT in vivo

We next assessed if the subpopulations we observed in vitro also exist in human adipose tissue. We compared our data set with a published snRNA-seq dataset derived from human BAT; hereafter called the "*BAT in vivo dataset*". As BAT contains multiple cell types, we first aimed to define a subpopulation within the dataset containing developing adipocytes, which could be compared with our single-cell dataset of human adipocytes. Therefore, we utilized the expression of two transcription factors important in brown adipogenesis, *PPARG* and *EBF2,* which were expressed in developing brown adipocytes in all three branches (progenitor, lower and upper), while highest expression was observed in the metabolic subpopulation (**Figure 2a**). We labeled the *EBF2* and *PPARG* expressing cells in cell atlases of the BAT in vivo dataset (**Figure 2b, top**) and labelled the sum of these cells (**Figure 2b**). We next performed a Seurat data integration using the in vitro adipocyte dataset containing P, U and L branches as reference to predict cell labels for the BAT in vivo dataset. Convincingly, we identified populations of all three branches (P, U, L) in the human BAT dataset among the cells that were predicted to be developing adipocytes based on *PPARG* and *EBF2* gene expression (**Figure 2c**). Interestingly, in vivo, *EBF2* expressing cells were mainly (but not exclusively) clustering with the L branch cells, whereas in vitro we observed higher *EBF2* expression in the U branch cells, raising the possibility of a switch between cell fates during adipogenesis. In support of the recapitulation of the P, U and L cell branches in the human BAT dataset, we validated this analysis using the Harmony algorithm[30], which confirmed our conclusion (**Figure 2d**).

Adipocyte progenitors split into structural and metabolic cell fates

We next explored the characteristics of the two identified cell-types by using BEAM[31], a bioinformatic approach to identify branch-dependent genes (**Table S4**). We identified six gene clusters of branch-dependent genes with distinct kinetic expression profiles (**Figure 3a**). The U branch was for example characterized by *ADIPOQ* encoding Adiponectin, a major regulator of lipid metabolism and insulin sensitivity[32], and mitochondrial uncoupling protein 2 (*UCP2*) (**Figure 3b**). *UCP2* is structurally in family with the brown fat specific, thermogenic gene *UCP1.* The L branch was characterized by genes encoding locally secreted proteins. This included *DCN*, encoding Decorin, an extracellular matrix protein, and *APOD*, encoding Apolipoprotein D, which is also present in the extracellular region and is a component of high-density lipoprotein (**Figure 3b**). Decorin has previously been reported to counteract adipogenesis[33]. To validate and visually examine the separation of the two cell fates within single cell cultures, we next performed FISH analyses, using RNAscope probes. As predicted, we observed a clear separation between our main markers, *ADIPOQ* and *DCN*, as well as between *ADIPOQ* and *APOD* expressing cells, whereas *ADIPOQ* and *UCP2* expressing cells were overlapping as expected (**Figure 3c**). Following the confirmation that *UCP2* was in the U branch, we assessed its co-localization with mitochondria in human brown adipocytes harvested at T5. We observed that cells highly abundant for the mitochondrial marker mtHSP70 were also positive for *UCP2* mRNA (**Figure 3d**). Whereas UCP2 has not been demonstrated to rescue thermogenic function in *UCP1* knockout mice[34], the protein is located in the mitochondrial inner membrane, allowing for Ca^{2+} to enter the mitochondria. The role of UCP2 in human BAT is to date

unexplored and several examples of species differences in thermogenic regulation exist[35,36]. We here show that it is the highest expressed *UCP* halfway through full maturation of human adipocytes (**Figure 3d**). To investigate if any of the cell fates demonstrated higher expression of thermogenic gene signature, we next grouped the cells by each branch, divided them into pseudotime deciles, and utilized the BATLAS[37] tool to predict brown and white adipocyte content (**Figure 3d**, **Table S6**). BATLAS is a computational prediction model for identifying brown versus white fat signatures in samples of unspecified content. Strikingly, we found that the U branch cells from all four depots, i.e. both BAT and WAT, were predicted to gradually develop into brown adipocytes in a pseudotime-dependent manner, while L the branch cells developed in the opposite direction (**Figure 3d**). This observation raised the idea that adipogenic cells exhibit a multipotent state halfway through full maturation, and that further thermogenic differentiation proceeds dependent on the adipose microenvironment.

This interpretation was consistent with a gene ontology analysis including all BEAM clusters that defined the U and L branches. Multiple genes encoding proteins localizing to the mitochondria and being part of lipid metabolism and the respiratory chain accumulated in the U branch (**Figure 3e**, **Table S5**). On the other hand, the L branch was clearly associated with an accumulation of processes related to extracellular matrix formation and developmental processes, including cellular adhesion (**Figure 3e, Table S5**). To reflect their predicted functions, we named the U branch cells "*Metabolic cells*" and the L branch cells "*Structural cells*".

.

Transcriptional network defining the metabolic and the structural cell types

To assess what defined the metabolic and the structural cell fates during differentiation, we next explored the landscape of transcription factors expression in pseudotime, identifying TFs with increasing branch-specific expression over pseudotime as drivers of branch development (**Figure 4a, Table S7**). The metabolic cells were defined by a well-established adipogenic transcription factor program[38]. This included Peroxisome proliferator-activated receptor gamma (PPAR-γ) and CCAAT/enhancer-binding protein alpha (C/EBPα), transcriptional activators that have been shown to synergistically activate adipogenesis by controlling genes important for adipocyte metabolism, including *CIDEC*, *PLIN1*, *CD36* and *ACSL1*[38] all of which were also defining the metabolic cells with higher expression compared to the structural cells. Additional transcription factors selective for the metabolic branch were *SREBF1* and *NR1H3*, stimulators of lipogenesis[39,40]. Intriguingly, the structural cells induced a transcriptional program driving osteogenic proliferation and differentiation. This program included *SNAI2* and *JUNB*, both promoting osteoblast maturation and forming a transcription factor network that counteracts adipogenesis[7]. Hence, the structural cells represent a cellular subpopulation that differentiates in a separate direction despite the addition of an adipogenic cocktail. These cells might be more involved in creating an adipose "skeleton", supporting the continuous adaptation of adipocyte size and structure by

adjusting the extracellular matrix. To validate and visualize the separation between the selective transcription factors for the metabolic and structural cells at T5 of human brown adipocytes we performed a FISH analysis using RNAscope probes. We found a clear separation between several transcription factors including the metabolic transcription factors *SREBF1* and *NR1H3* versus the structural *PRRX1*, and the metabolic transcription factors *PPARG* and *CEBPA* versus the structural *SNAI2* (**Figure 4a**). We co-stained for additional branching transcription factors, demonstrating a similar cell population separation, with the exception of JUNB and PPARG that seemed to co-localize (**Figure S9**). By taking advantage of our pseudotime-ordered dataset and applying a novel tool called Scellnetor[41] we were able to identify transcriptional networks involving a subset of the metabolic branch selective transcription factors (**Figure 4b**). Scellnetor is designed to identify gene networks enriched in differentiation trajectories[41]. This network analysis identified additional genes in the metabolic transcription factor networks including *PPARGC1A*, *PPARGCIB*, *CIDEA* and *CKMT1B*, further emphasizing the metabolic nature of this branch[42]. We next assessed whether there were any differences in the transcription factor dynamics between brown and white adipocytes. We grouped cells derived from supraclavicular and perirenal brown adipose depot into the “BAT” group and the cells derived from subcutaneous and visceral white adipose into the “WAT” group, and compared the pseudotime windows at which transcription factors diverged in expression between the metabolic and structural branches (**Figure 4c**). For example, we found that *EBF2*, a transcription factor well described for promoting brown adipogenesis[43] defined the metabolic branch in brown adipocytes only, and rather early in pseudotime. However, most differences between brown and white adipocytes became clear later in pseudotime, for example *RXRG*, which also defined the metabolic branch in brown adipocytes only. *RXRG* acts as a co-transcription factor with *PPARG* to promote thermogenic gene transcription[42] (**Figure 4c**). Among the genes defining the structural branch were the above-mentioned *SNAI2* and *JUNB*, driving this branch in both brown and white adipocytes. Interestingly, in late pseudotime, we observed *NFIA*, a structural branch-selective gene in brown adipocytes only, previously reported to promote the brown fat differentiation program[44] (**Figure 4c**). By predefining the cell origin from either brown or white adipose depots before sorting into pseudotime, we were thus able to identify branch-specific transcription factors within brown or white adipocytes (**Figure 4d**). Some of these brown or white selective transcription factors are previously described in bulk data[24,42,44], whereas several are novel and might prove powerful as directors of the brown and white adipocyte differentiation programs, respectively.

The Metabolic cell branch associates with traits for waist/hip ratio

To investigate the relevance of our cultured cells in human health and disease, we used the computational tool CELLECT[45], to genetically prioritize our pseudo-temporal ordered data for relevant human traits. Briefly, CELLECT quantifies the association between the expression patterns of cell-types and the genetic components of human complex traits identified by genome-wide association studies (GWAS). CELLECT tests for enrichment of genetic association signal for single nucleotide

polymorphisms (SNPs) proximal to genes specifically expressed in each cell-type. For this analysis, we delineated cell populations by stratifying cells by pseudotime decile for each developmental branch, generating 30 strata of cells. These cells from each strata were then used as input to CELLECT to estimate expression specificity of genes in any of these groups. We performed CELLECT analysis for 39 GWAS traits (**Table S8**). We identified significant enrichment of genetic association signal for cell populations in the U branch for fat distribution (as assessed by waist-to-hip ratio (WHR) and WHR adjusted for BMI (WHRadjBMI)), and lipid levels (as assessed by low-density lipid levels) (**Figure 5b**, **Table S9**). Interestingly, the P and L branches displayed little or no enrichment. These results indicate that the branch point of adipogenesis, and the metabolic gene signature identified in this study is likely to be relevant for fat distribution and lipid metabolism. As a control of the model, we assessed the genetic enrichment for height and BMI GWAS and found no enrichment, consistent with the expectation that adipogenic development does not impact human height. Neither did we find enrichment for any of the remaining GWAS traits analyzed, underscoring the strong impact of inducing the metabolic cell fate for determining fat distribution in humans. To understand the function and crosstalk between these two cell types, we predicted their cell-type specific secretomes ordered by pseudotime. We utilized the published human secretome[46] as a scaffold to predict a secreted product from the branch specific genes. We performed separate analyses for cells derived from BAT (supraclavicular and perirenal) and WAT (subcutaneous and visceral). In the metabolic cells, expression of several humanin-like peptides encoded by MTRNR2L1, MTRNR2L8, MTRNR2L10 and MTRNR2L12 caught our attention. These peptides are transcribed from the nucleus as homologues to the mitochondrial microprotein, humanin. They are transcribed from different chromosomes and include humanin-like 1, 8, 10 and 12 (**Figure 5c**). Humanin and the humanin-like peptides are 24 amino acid long peptides. Humanin associates with cardiometabolic function[47] and is regulated by IGF-1. Interestingly, IGF-1 is expressed from the structural branch raising the idea of a direct crosstalk between the branches. The structural cells encoded multiple extracellular matrix factors annotated as secreted. Among many others, these included several types of collagens and fibronectin, proteins that are highly abundant in the development of obesity-induced fibrosis[48] (**Figure 5d**). The secreting capacity of the structural cells were underscored by the outnumbering of the secreting factors defining the metabolic cells, with around double the amount of genes encoding secreted products in the structural cell compared to the metabolic cells (**Figure 5e**).

Discussion

We here investigate the first phase of adipogenesis at single cell resolution across cells derived from four different human BAT and WAT depots. We use single cell trajectory analysis, creating a continuous gene signature using pseudotime analysis. We demonstrate that two cell fates arise from the same progenitor cells. This split occurs during the onset of differentiation and divides the cells into a metabolic and a structural cell type. Halfway through full differentiation, the metabolic cell type expresses a gene signature reflecting multiple metabolic pathways and a brown fat phenotype, regardless of BAT or WAT origin. The metabolic cellular gene signature is associated with genetic variants associated with body for

fat distribution. The structural cells express developmental and extracellular matrix genes, many of which are upregulated during obesity-induced adipose tissue fibrosis.

Our findings suggest a competing balance between two cell fates with complementing roles in the adipose tissue architecture and function. Importantly, previous studies have proposed that adipocyte progenitors can take on either a fibrogenic or an adipogenic path[49]. In the current study, we find that these cell fates correspond to a structural and a metabolic cell type present in differentiating adipocytes from four different white and brown adipose depots of adult humans. These cell fates are thus closely related and interestingly their branching transcription factor signatures aligns with a previously described transcription factor network shared between adipocytes and osteoblasts[7]. This network controls a switch between differentiation into either cell type[7]. The authors demonstrated that suppression of the osteoblast transcription factor network allowed the cells to differentiate into adipocytes, and this was possible upon the induction of *PPARG*[7]. In the light of the data from Rauch and co-authors, our current results strongly suggest that the structural and the metabolic cell type arise from the same progenitor cells and that the cell fate is determined by asymmetric regulation of an adipocyte/osteoblast transcription factor network. These findings raise the hypothesis of a closer interaction between these two cell types within the adipose tissue than previously anticipated, arguing for that this interaction should be taken into account when targeting obesity and metabolic disease. Interestingly, a specific cell type that actively inhibits adipogenesis have been described in previous studies at single cell resolution[14]. Others have demonstrated a subtype of adipocyte progenitors spatially associated with fibrotic structures and macrophages[12]. Importantly, the extracellular matrix provides a niche for the adipocytes and has been reported to affect the adipocytes to such an extent that cells stripped and swapped from the extracellular matrix of visceral versus subcutaneous adipocytes resulted in a phenotype corresponding to the origin of the extracellular matrix[33]. Moreover, a comparative secretomics study mapped a distinct extracellular matrix proteome between human brown and white adipocytes[50], further supporting a role of extracellular matrix in defining adipocyte characteristics. These observations support the idea of two contradicting cell fates, a structural-fibrogenic and an metabolic-adipogenic fate, with a balance between these two cell fates that can be shifted by external factors in the adipose microenvironment.

The metabolic cell type displayed a brown adipocyte signature, an intriguing finding, as this cell type was also common among the cells originating from WAT and BAT. Importantly, this finding can provide an explanation of the literature during the last decade describing browning of WAT, a process on differentiation of thermogenic adipocytes within WAT[51]. The phenomenon of thermogenic differentiation in WAT was first described through induction of *PPARG* during in vitro differentiation of murine epididymal adipocytes by adding pharmacological doses of rosiglitazone[52]. At the same time, *PPARG* is a well-described adipogenic transcription factor also essential for differentiation of white adipocytes[53].

Taken together with our current findings, these data suggest that the thermogenic signature is present at a premature state in all adipocytes, but restricted in the later maturation of white adipocytes, perhaps through WAT-specific interactions between the co-differentiating metabolic and structural cells. Our data also brings perspective to previous findings that beige adipocytes within WAT initially arise from environmentally primed progenitors, giving rise to de novo beige adipogenesis of adipocytes that subsequently can interconvert between a dormant and an active state[54,55]. Taken together, these observations underscore the thermal plasticity of adipose tissue and the capacity to adapt to environmental temperatures.

As we here show that the metabolic cells are present in all adipose depots and associate with common genetic variants associated with waist-to-hip ratio adjusted for BMI, it is relevant to discuss how metabolic/structural cell fate proportion could affect hip/waist ratio and metabolic health. If the metabolic cell gene signature fails to induce differentiation of a proper metabolic cell phenotype due to the associating SNPs, this would affect the metabolic cells across all BAT and WAT adipose depots in the body. Given the brown adipocyte signature of the metabolic cells, a reduced proportion would likely result in less thermogenic capacity in the BAT depots. In the subcutaneous WAT depots, it would likely result in reduced capacity for safe lipid storage, which in turn could result in an increased ectopic fat deposition in the viscera. Taken together, we find that the metabolic gene signature associates with genetic variations for fat distribution, and this might in turn provide a common explanation to associations between unfavorable metabolic health and hip/waist ratio on one hand[1], and BAT activity and cardiometabolic health on the other hand[56]. In support of this notion, we previously observed that UCP1 expression in human BAT directly correlates with waist/hip ratio[57].

In conclusion, we here provide a seamless differentiation map of progenitor cells from four human BAT and WAT depots, revealing two main cell fates across all depots. Our data challenge the current conception of the origins of adipogenic and fibrogenic adipose resident cells and provides a missing piece of the puzzle for understanding browning of WAT. From a larger perspective, our data set the base for targeting obesity and its related diseases at a single cell specific level.

Declarations

Acknowledgements

We thank Birgitte R. Lisdorf, Maren Schrölkamp, Therese Juhlin Larsen, Neha Mathur, Peter Sandbeck and Tina Hvidtfeldt Lorentzen for their technical assistance. We thank Julie Lee and the Single Cell Omics platform at CBMR, and Romain Barrés for providing the RNA sequencing. Novo Nordisk Foundation Center for Basic Metabolic Research is an independent Research Center, based at the University of Copenhagen, Denmark and partially funded by an unconditional donation from the Novo Nordisk

Foundation (www.cbmr.ku.dk) (Grant number NNF18CC0034900). The Centre for Physical Activity Research (CFAS) is supported by a grant from TrygFonden. During the study period the Centre for Inflammation and Metabolism (CIM) was supported by a grant from the Danish National Research Foundation (DNRF55). THP acknowledges the Novo Nordisk Foundation (Grant number NNF16OC0021496) and the Lundbeck Foundation (Grant number R19020143904). CS acknowledges Augustinusfonden (Grant number 17-4359), Novonordiskfonden Grant number: NNF15OC0017922 and Lundbeck foundation (Grant number 2013-13799). PNT acknowledges the Danish Ministry of Higher Education and Science for Elite Research PhD scholarship. NJ was supported by a research grant from the Danish Diabetes Academy, which is funded by the Novo Nordisk Foundation, grant number NNF17SA0031406. This project has received funding from the European Research Council (ERC) under the European Union's Horizon 2020 research and innovation programme (grant agreement No. [101002725]) (CS).

Author contributions

CS, SN and THP supervised the study. CS, SN, NP, THP and PNT designed the study. CS and SN lead experimental work, provided sample material, and biological hypotheses. NP, PNT and PF lead bioinformatic analysis; performed transcriptomics data analysis and visualizations. AG performed Scellnetor analysis. SN, TH and KDH performed RNA FISH. TH, LP, VHJ, KDH and NJ, performed cell experiments. CW and WS provided single nuclei data of brown adipose tissue. CS, SN, NP, PNT and PF interpreted the data and wrote the manuscript. All authors read and approved the manuscript.

Competing interests

The authors declare no competing interests.

Methods

Human samples

Human adipogenic progenitor cells were isolated from the stromal vascular fraction of the biopsies on the day they were obtained (surgery or biopsy), from the following four adipose regions: 1) visceral adipose tissue (obtained during gallbladder surgery); 2) perirenal adipose tissue (obtained during nephrectomy surgery); 3) abdominal subcutaneous adipose tissue (obtained with the Bergström needle biopsy method) and 4) supraclavicular adipose tissue (obtained during surgery in patients with suspected cancer in the neck area). Isolated cells were expanded and frozen in liquid nitrogen in a proliferative state as previously described[25] until the onset of the study. Data from the cohorts have previously been published[19,20,58]. All subjects provided written consent and the studies were performed in accordance with the declaration of Helsinki. The cell studies were approved by the Danish Data protection agency, Denmark, journal number RH-2017-69, I-Suite nr: 05329.

Cell culturing

Biopsies were collected in DMEM/F12 (Gibco) with 1% penicillin/streptomycin (Life Technologies) and tubes were kept on ice during transport. A detailed protocol for isolation and culturing of human adipocyte progenitors has been previously contributed[25]. Briefly, Biopsies were digested with 10 mg collagenase II (C6885-1G, Sigma) and 100 mg BSA (A8806-5G, Sigma) in 10 ml DMEM/F12 for 20 min at 37°C while gently shaken. Following digestion, the suspension was filtered, and cells were washed with DMEM/F12, resuspended in DMEM/F12, 1% PS, 10% fetal bovine serum (FBS) (Life Technologies) and seeded in a 25 cm^2 culture flask. Media was changed the day following isolation and then every second day until cells were 80% confluent; at this point, cultures were split into a 10 cm dish (passage 0). Cells were expanded by splitting 1:3. For the single-cell experiment, cells were seeded in 6 well plates in proliferation media consisting of DMEM/F12, 10% FBS, 1% PS and 1 nM Fibroblast growth factor-acidic (FGF-1) (ImmunoTools). Cells were grown at 37°C in an atmosphere of 5% CO_2 and the media was changed every second day. Adipocyte differentiation was induced two days after adipocyte progenitor cultures were 100% confluent by removal of FGF-1 from the media and addition of a differentiation cocktail (see details below) consisting of DMEM/F12 containing 1% PS, 0.1 µM dexamethasone (Sigma–Aldrich), 100 nM insulin (Actrapid, Novo Nordisk or Humulin, Eli Lilly), 200 nM rosiglitazone (Sigma–Aldrich), 540 µM isobutylmethylxanthine (Sigma–Aldrich), 2 nM T3 (Sigma–Aldrich) and 10 µg/ml transferrin (Sigma–Aldrich). After three days of differentiation, isobutylmethylxanthine was removed from the cell culture media and cells were differentiated for additional three days with the remaining differentiation compounds. For the 10x single-cell sorting, cells were loosened by adding 2 ml of TrypLex and placed in incubator for 3 min. Detachment of cells was confirmed by microscopy and 3 ml of Proliferation Media (PM) was added to the cells to inactivate trypsin. 190µl of cell-suspension was then transferred to an eppendorf-tube and mixed with 10µl of Solution 13 AO-DAPI, and then counted on a nucleocounter NC-3000. Cells were counted as described above, and 8000 cells/donor were pooled in an Eppendorf tube. The pool of cells was centrifuged for 7 min at 700g and resuspended in 80µl PBS with FFA-free BSA.

Single-cell library preparation and sequencing

Single-cell cDNA libraries were generated using Chromium Single Cell platform and 3’ v2 Reagent Kit according to manufacturer’s protocol (10x Genomics, USA). Single-cell libraries were sequenced on a NextSeq 500 platform to obtain 100 and 32-bp paired end reads using the following read length: read 1, 26 cycles, read 2, 98 cycles and i7 index, 8 cycles. CellRanger[59] (version 2.0.1) was used with default parameters to demultiplex and align reads to the hg19 reference genome, filter cell and UMI barcodes, and generate gene count matrices.

Genotyping

Samples were genotyped with Infinium Global Screening Array-24 v1.0 (Illumina). Genotypes for each individual were called using Illumina GenomeStudio (v2.0) with h19 as reference genome. We exported the genotype calls using the PLINK export plugin (PLINK Input Report Plug-in v2.1.4) and used the software HRC-1000G-check-bim (v4.2.9) to QC the 618,540 genotyped SNPs prior to imputation. The program matches strand, SNP ID names, positions, alleles, ref/alt assignment to 1000 Genome Project reference data. After QC 267,821 SNPs were retained. These SNPs (excluding the X-chromosome) were imputed using Minimac3 via the Michigan Imputation Server with default settings (EUR 1000G phase 3 v5 as reference panel and phasing using Eagle v2.3). Out of the 47,109,485 imputed SNPs, we retained 3,031,027 SNPs with high imputation quality (R2 > 0.8) and MAF > 0.2.

Genotyping and Demuxlet sample identity deconvolution

The Demuxlet algorithm[60] allows for genetic deconvolution of sample identity and doublet detection in single-cell libraries with samples pooled across individuals. We used Demuxlet (version 1.0, download data Jul 25, 2018) and genotypes obtained as described above to deconvolute sample identity in our cell libraries. As recommended by the authors of Demuxlet, we filtered out SNPs in non-exonic regions (defined by GENCODE release 19), retaining 93,898 SNPs, prior to running Demuxlet. The average number of SNPs per cell reported by Demuxlet was 127 (counting cells in the Cell Ranger filtered matrices). We discarded 3,444 cells (12.8 % of total) identified by Demuxlet as doublets (**Supplementary Tables file, sheet 10**).

Proliferating adipocyte analysis

We used the R package Seurat[61] for pre-processing the data, quality control, regression of cell cycle effects, sample alignment and differential expression analyses. We performed quality control on our data to filter out low quality cells and genes, and we preprocessed the data to the format required for further analysis. As all proliferating adipocyte progenitors could be expected to have similar mitochondrial content, we filtered out cells where the mitochondrial gene expression was higher than 8%, as deviating high mitochondrial gene expression indicates stressed cells. Cells with less than 200 genes or more than 9,000 genes were also removed, as well as cells with more than 120,000 UMI's to remove possible

doublets. The filtered data was log normalized and scaled, and the number of UMI's and percentage of mitochondrial genes were subsequently regressed out of the data. PCA was performed on the data and the first 15 PC's were used for clustering and t-SNE visualization. Each cell was then scored for cell cycle phase. Please find all details on the computational analyses at https://github.com/scheelelab/10x-adipocyte-analysis

Seurat

We used the R package Seurat[61] (version 2.3.4) for preprocessing the data, quality control and differential expression analyses. As input to Seurat, we used the digital gene expression matrix output from the 10x Genomics analysis pipeline CellRanger. Cells with less than 200 genes and genes expressed in less than 3 cells were filtered out. The percentage of mitochondrial gene expression was calculated for each cell. However, as mitochondrial gene expression increase during adipogenesis, we did not exclude cells with high mitochondrial expression in the developing adipocyte progenitor data set. We performed principal component analysis (PCA) to compute principal components (PCs) needed for clustering and data visualization. PC's were computed on the highly variable genes identified on log normalized and scaled data. Clusters were identified using a shared nearest neighbor (SNN) modularity optimization-based clustering algorithm, which takes as input the significant number of PC's. The data was visualized using Seurat's implementation of t-distributed stochastic neighbor embedding[62] (t-SNE).

Monocle

We used the R tool Monocle[63] (version 2.8.0) to construct the cell developmental trajectory of the preprocessed Seurat object. Feature selection for trajectory construction was performed as follows: first the dataset was split into two subsets, one containing all cells from T1, T2 and T3 and one containing all cells from T4 and T5. Both subsets were then clustered using Seurat's default clustering algorithm with a resolution of 1.5. Differential expression tests were performed for every cluster against the rest of the cells in the subset (using the negative binomial test, filtering on absolute logFC > 0.25). The union of the resulting gene list (2,464 genes) was used as input feature list for building the Monocle trajectory (DDRTree algorithm, max_components = 2). Monocle orders cells by pseudotime along the trajectories. (Pseudotime is an abstract unit of progress: it is the distance between a cell and the start of the trajectory, measured along the shortest path. The trajectories total length is defined in terms of the total amount of transcriptional change that a cell undergoes as it moves from the starting state to the end state.) We used Monocle's Branched Expression Analysis Modeling[64] (BEAM) to identify branch dependent genes. The genes in the resulting list were filtered on q-value < 0.05 (8,647 genes remaining) and subsequently filtered on absolute average logFC > 0.3 between the U branch and L branch (413 genes remaining). To subset transcription factors in the BEAM analysis, we retrieved the gene type, GO term name and GO term

definition for every gene in our dataset using Ensembl Biomart (version 96). From this set of annotated genes, we created two gene sets: a transcription factor gene set by selecting genes annotated with the 'transcription factor' GO term, and a non-coding gene set by filtering out genes annotated with the gene type 'protein_coding'.

Velocyto

We ran the Velocyto[65] command line tool for every sample with a genome annotation file and expressed repeat annotation file (reference genome hg19). We used the Python library for further downstream analysis. First the loom files of every sample were aggregated into one. Cells that were not present in the final Seurat analysis were discarded and the metadata from the Seurat analysis was added to the remaining cells. We further discarded cells with extremely low unspliced detection, keeping 23,309 cells for the final analysis. Genes were filtered by ranking the spliced genes based on a coefficient of variation vs. mean fit, using the top 3000 to perform a PCA. Both the spliced and the unspliced gene expression matrices were subsequently normalized by size. Using the first 15 principal components, the data was kNN-smoothed (using the default value of k; 0.025 x nCells). The standard implementation of Velocyto was used with default parameters for fitting gene models, predicting velocity, extrapolating and plotting.

Gene set enrichment analyses

Gene set enrichment analyses were performed using the R package gProfileR[66]. GProfileR takes as input a list with gene symbols and returns a table with terms associated with those genes. We filtered the output to only contain Gene Ontology (GO) terms. To generate the figure with GO terms we performed gene set enrichment analyses on every cluster of branch-dependent genes identified using BEAM (6 clusters, 413 genes in total, absolute log fold-change > 0.3 between U branch and L branch). The resulting GO terms and their p-values were used as input for REViGO[67], a web tool to summarize lists of GO terms by removing redundant terms. To visualize the summarized GO terms associated with branch-dependent genes, we used the R package GOplot[68]. GOplot calculates a z-score for each GO term indicating if the term is more likely to be decreased (negative value) or increased (positive value): , where *up* and *down* are the number of up- and down-regulated genes, respectively, counting genes with log fold-change > 0 between the U and L branch as up-regulated genes.

BATLAS

We used the webtool BATLAS[37] to predict the percentage of brown adipocyte content in our data. We grouped cells from each Monocle developmental branch (progenitor, lower and upper) by pseudotime decile, to generate 30 groups of cells. The average expression for every gene in each decile was subsequently calculated on the normalized data in non-log space. The resulting matrix was used as input for BATLAS.

Branch-specific gene expression analysis in pseudotime.

Lists of human transcription factors[69] and of the human secretome[46] were used as input for identifying branch-specific gene expression over pseudotime. For each gene, smoothed gene expression across cells along pseudotime was determined, and the pseudotime point at which expression increases in one branch compared to the other was identified. To be considered as a valid result, we required that genes that were identified as diverging in expression between branches maintained the trend of divergence until end of pseudotime.

Genetic prioritization analysis

We used CELLECT [**CELL**-type **E**xpression-specific integration for **C**omplex **T**raits][70] to genetically prioritize pseudo-temporal ordered groups of cells. Specifically, we grouped cells from each Monocle developmental branch (progenitor, lower and upper) by pseudotime decile, to generate 30 groups of cells. We used CELLEX [**CELL**-type **EX**pression-specificity][70] to calculate expression specificity of these cell groups. Briefly, CELLEX normalizes the expression data using a common transcript count (assuming 10,000 transcripts per cell) and apply log-transformation. Next expression specificity likelihood (ES_μ) is computed for groups of cells. We used CELLECT with S-LDSC[71] as the genetic prioritization model. We ran CELLECT with default parameters (100 kb window size around each gene, correcting for baseline v1.1 and 'all genes' annotations, see Timshel2019[70] for details). We performed CELLECT analysis for **39** GWAS traits listed in **Supplementary Table file, sheet 8**.

RNA Fluorescent in Situ Hybridization

In vitro differentiated human adipocytes derived from either subcutaneous or supraclavicular deep neck adipose depots were fixed at day 4 and 6 of differentiation with 10% neutral buffered formalin (Thermo Fisher Scientific) for 30 minutes, dehydrated and stored in 100% ethanol until the staining procedure. In situ hybridization was performed using RNAscope Fluorescent Multiplex Plex v2 Reagent Kit and RNAscope manual assay probes designed and produced by Advanced Cell Diagnostics (ACD). Nuclei were stained with NucBlue ReadyProbes (Thermo Fisher Scientific). RNA targets were visualized using an EVOS imaging system (Thermo Fisher Scientific). The RNA targets were hybridized with RNAscope

probes (table S11) and then labelled with the Opal 570, Opal 620 and Opal 690 (Akoya Biosciences). The fluorescent signals were detected with an RFP, Cy5 and Texas red light cubes.

Validation of L and U branch cell-fates in human single-nucleus tissue

We obtained human deep neck BAT single-nucleus RNA-seq data[72]. The dataset comprises 50,284 cells from a total of 16 individuals. Cells were profiled using 10x Chromium V3. We applied standard Seurat workflow (as described previously) to QC and cluster the cells. We used Seurat v3[73] to integrate and transfer cell labels from our developmental adipocyte progenitors (T1-T5) to the Wolfrum group dataset. Briefly, this approach consists of identifying 'cell anchors' between datasets that can then be used to harmonize the datasets and transfer information from one dataset to another. We used the functions FindTransferAnchors(reference= adipocyte progenitors_T1-T5, query=wolfrum_group_BAT) and TransferData() with default parameters to identify anchors and transfer P, U and L cell labels to Wolfrum group data. We retained only high confident transferred labels with a transfer score above 0.7 (the transfer score ranges between 0-1, where increasing values indicate the confidence of the transfer) and labeled all other cells as 'non-matching cells'.

Data repository and code availability

All processed RNA sequencing data is deposited in ArrayExpress: E-MTAB-XXX and E-MTAB-XXX.

The source code to reproduce all figures and tables for this manuscript are available at

https://github.com/scheelelab/10x-adipocyte-analysis

URLs

1. Cell Ranger: https://support.10xgenomics.com/single-cell-gene-expression/software/pipelines/latest/what-is-cell-ranger
2. Michigan Imputation Server : https://imputationserver.sph.umich.edu/index.html
3. HRC-1000G-check-bim.pl: http://www.well.ox.ac.uk/~wrayner/tools/#Checking
4. Demuxlet: https://github.com/statgen/demuxlet
5. Seurat: https://github.com/satijalab/seurat
6. Monocle: https://github.com/cole-trapnell-lab/monocle-release
7. gProfileR: https://biit.cs.ut.ee/gprofiler/gost

8. BATLAS: http://green-l-12.ethz.ch:3838/BATLAS/
9. REVIGO: http://revigo.irb.hr/
10. GOplot: https://wencke.github.io/

References

1. Karpe, F. & Pinnick, K. E. Biology of upper-body and lower-body adipose tissue-link to whole-body phenotypes. *Nature reviews. Endocrinology* **11**, 90–100 (2014).

2. Zammouri, J. *et al.* Molecular and Cellular Bases of Lipodystrophy Syndromes. *Frontiers in Endocrinology* **12**, (2022).

3. Pellegrinelli, V., Carobbio, S. & Vidal-Puig, A. Adipose tissue plasticity: how fat depots respond differently to pathophysiological cues. *Diabetologia* vol. 59 1075–1088 (2016).

4. Scheele, C. & Nielsen, S. Metabolic regulation and the anti-obesity perspectives of human brown fat. *Redox Biology* **12**, 770–775 (2017).

5. Almalki, S. G. & Agrawal, D. K. Key transcription factors in the differentiation of mesenchymal stem cells. *Differentiation* vol. 92 41–51 (2016).

6. Timmons, J. A. *et al.* Myogenic gene expression signature establishes that brown and white adipocytes originate from distinct cell lineages. *Proceedings of the National Academy of Sciences of the United States of America* **104**, 4401–4406 (2007).

7. Rauch, A. *et al.* Osteogenesis depends on commissioning of a network of stem cell transcription factors that act as repressors of adipogenesis. *Nature Genetics* **51**, 716–727 (2019).

8. Fink, T. *et al.* Adipose-derived stem cells from the brown bear (Ursus arctos) spontaneously undergo chondrogenic and osteogenic differentiation in vitro. *Stem Cell Research* **7**, 89–95 (2011).

9. Corvera, S. Cellular Heterogeneity in Adipose Tissues. *Annual Review of Physiology* **83**, 257–278 (2021).

10. Raajendiran, A. *et al.* Identification of Metabolically Distinct Adipocyte Progenitor Cells in Human Adipose Tissues. *Cell Reports* **27**, 1528-1540.e7 (2019).

11. Scheele, C. & Wolfrum C. Functional diversity of human adipose tissue revealed by spatial mapping. *Nature reviews. Endocrinology* (2021) doi:10.1038/S41574-021-00582-2.

12. Bäckdahl, J. *et al.* Spatial mapping reveals human adipocyte subpopulations with distinct sensitivities to insulin. *Cell Metabolism* **33**, 1869-1882.e6 (2021).

13. Min, S. Y. *et al.* Diverse repertoire of human adipocyte subtypes develops from transcriptionally distinct mesenchymal progenitor cells. *Proceedings of the National Academy of Sciences of the United States of America* **116**, (2019).

14. Schwalie, P. C. *et al.* A stromal cell population that inhibits adipogenesis in mammalian fat depots. *Nature* **559**, 103–108 (2018).

15. Søberg, S. *et al.* Altered brown fat thermoregulation and enhanced cold-induced thermogenesis in young, healthy, winter-swimming men. *Cell Reports Medicine* **2**, (2021).

16. Søndergaard, E. *et al.* Chronic adrenergic stimulation induces brown adipose tissue differentiation in visceral adipose tissue. *Diabetic Medicine* **32**, e4–e8 (2015).

17. Frontini, A. *et al.* White-to-brown transdifferentiation of omental adipocytes in patients affected by pheochromocytoma. *Biochimica et biophysica acta* **1831**, 950–959 (2013).

18. Sidossis, L. S. *et al.* Browning of Subcutaneous White Adipose Tissue in Humans after Severe Adrenergic Stress. *Cell Metabolism* **22**, 219–227 (2015).

19. Jespersen, N. Z. *et al.* Heterogeneity in the perirenal region of humans suggests presence of dormant brown adipose tissue that contains brown fat precursor cells. *Molecular Metabolism* (2019) doi:10.1016/J.MOLMET.2019.03.005.

20. Jespersen, N. Z. N. Z. *et al.* A classical brown adipose tissue mrna signature partly overlaps with brite in the supraclavicular region of adult humans. *Cell Metabolism* **17**, 798–805 (2013).

21. Xue, R. *et al.* Clonal analyses and gene profiling identify genetic biomarkers of the thermogenic potential of human brown and white preadipocytes. *Nature medicine* **21**, 760–768 (2015).

22. Kiselev, V. Y., Yiu, A. & Hemberg, M. Scmap: Projection of single-cell RNA-seq data across data sets. *Nature Methods* **15**, 359–362 (2018).

23. Schaum, N. *et al.* Single-cell transcriptomics of 20 mouse organs creates a Tabula Muris. *Nature* **562**, 367–372 (2018).

24. Wang, W. & Seale, P. Control of brown and beige fat development. *Nat Rev Mol Cell Biol.* **17**, 691-702. (2016).

25. Larsen, T. J., Jespersen, N. Z. & Scheele, C. Adipogenesis in Primary Cell Culture. in *Handbook of Experimental Pharmacology* vol. Jul 7 (2018).

26. Trapnell, C. *et al.* The dynamics and regulators of cell fate decisions are revealed by pseudotemporal ordering of single cells. *Nature Biotechnology* **32**, 381–386 (2014).

27. Chen, J. *et al.* Clonal mature adipocyte production of proliferative-competent daughter cells requires lipid export prior to cell division. *International Journal of Stem Cells* **2**, 76–78 (2009).

28. Giordano, A., Smorlesi, A., Frontini, A., Barbatelli, G. & Cint, S. White, brown and pink adipocytes: The extraordinary plasticity of the adipose organ. *European Journal of Endocrinology* **170**, (2014).

29. He, X. *et al.* RNA velocity of single cells. *Nature* **560**, 494–498 (2018).

30. Korsunsky, I. *et al.* Fast, sensitive and accurate integration of single-cell data with Harmony. *Nature methods* **16**, 1289–1296 (2019).

31. Qiu, X. *et al.* Single-cell mRNA quantification and differential analysis with Census. *Nature Methods* **14**, 309–315 (2017).

32. Yamauchi, T. *et al.* The fat-derived hormone adiponectin reverses insulin resistance associated with both lipoatrophy and obesity . PubMed Commons. 1–2 (2014).

33. Meissburger, B. *et al.* Regulation of adipogenesis by paracrine factors from adipose stromal-vascular fraction - a link to fat depot-specific differences. *Biochimica et Biophysica Acta - Molecular and Cell Biology of Lipids* **1861**, 1121–1131 (2016).

34. Nedergaard, J. *et al. UCP1: the only protein able to mediate adaptive non-shivering thermogenesis and metabolic ine□ciency*. www.elsevier.com/locate/bba.

35. Blondin, D. P. *et al.* Human Brown Adipocyte Thermogenesis Is Driven by β2-AR Stimulation. *Cell Metabolism* **32**, 287-300.e7 (2020).

36. Tran, K. van *et al.* Human thermogenic adipocyte regulation by the long noncoding RNA LINC00473. *Nature Metabolism* **2**, 397–412 (2020).

37. Perdikari, A. *et al.* BATLAS: Deconvoluting Brown Adipose Tissue. *Cell Reports* **25**, 784-797.e4 (2018).

38. Madsen, M. S., Siersbaek, R., Boergesen, M., Nielsen, R. & Mandrup, S. Peroxisome Proliferator-Activated Receptor and C/EBP Synergistically Activate Key Metabolic Adipocyte Genes by Assisted Loading. *Molecular and Cellular Biology* **34**, 939–954 (2013).

39. Schultz, J. R. *et al.* Role of LXRs in control of lipogenesis. *Genes and Development* **14**, 2831–2838 (2000).

40. Song, Z., Xiaoli, A. M. & Yang, F. Regulation and metabolic significance of De Novo lipogenesis in adipose tissues. *Nutrients* vol. 10 (2018).

41. Grønning, A. G. B. *et al.* Enabling single-cell trajectory network enrichment. *Nature Computational Science* **1**, 153–163 (2021).

42. Loft, A., Forss, I. & Mandrup, S. Genome-Wide Insights into the Development and Function of Thermogenic Adipocytes. *Trends in Endocrinology & Metabolism* **28**, 104–120 (2017).

43. Wang, W. *et al.* Ebf2 is a selective marker of brown and beige adipogenic precursor cells. *Proceedings of the National Academy of Sciences* **111**, 14466–14471 (2014).

44. Hiraike, Y. *et al.* NFIA co-localizes with PPARγ and transcriptionally controls the brown fat gene program. *Nature Cell Biology* **19**, 1081–1092 (2017).

45. Timshel, P. N., Thompson, J. J. & Pers, T. H. Genetic mapping of etiologic brain cell types for obesity. *eLife* **9**, (2020).

46. Uhlén, M. *et al.* The human secretome. *Science Signaling* **12**, (2019).

47. Rochette, L. *et al.* Mitochondrial-derived peptides: New markers for cardiometabolic dysfunction. *Archives of Cardiovascular Diseases* **115**, 48–56 (2022).

48. Ruiz-Ojeda, Méndez-Gutiérrez, Aguilera & Plaza-Díaz. Extracellular Matrix Remodeling of Adipose Tissue in Obesity and Metabolic Diseases. *International Journal of Molecular Sciences* **20**, 4888 (2019).

49. Sakers, A., de Siqueira, M. K., Seale, P. & Villanueva, C. J. Adipose-tissue plasticity in health and disease. *Cell* **185**, 419–446 (2022).

50. Deshmukh, A. S. *et al.* Proteomics-Based Comparative Mapping of the Secretomes of Human Brown and White Adipocytes Reveals EPDR1 as a Novel Batokine. *Cell Metabolism* (2019) doi:10.1016/j.cmet.2019.10.001.

51. Seale, P. *et al.* Prdm16 determines the thermogenic program of subcutaneous white adipose tissue in mice. *Journal of Clinical Investigation* **121**, 96–105 (2011).

52. Petrovic, N. *et al.* Chronic peroxisome proliferator-activated receptor gamma (PPARG) activation of epididymally derived white adipocyte cultures reveals a population of thermogenically competent, UCP1-containing adipocytes molecularly distinct from classic brown adipocytes. *Journal of Biological Chemistry* **285**, 7153–7164 (2010).

53. Siersbæk, R., Nielsen, R. & Mandrup, S. PPARγ in adipocyte differentiation and metabolism - Novel insights from genome-wide studies. *FEBS Letters* **584**, 3242–3249 (2010).

54. Shao, M. *et al.* Cellular Origins of Beige Fat Cells Revisited. *Diabetes* **68**, 1874–1885 (2019).

55. Rosenwald, M., Perdikari, A., Rülicke, T. & Wolfrum, C. Bi-directional interconversion of brite and white adipocytes. *Nature Cell Biology* **15**, 659 (2013).

56. Becher, T. *et al.* Brown adipose tissue is associated with cardiometabolic health. *Nature Medicine* **27**, 58–65 (2021).

57. Jespersen, N. Z. *et al.* Thermogenic genes are blunted whereas brown adipose tissue identity is preserved in human obesity. *bioRxiv* 2020.05.07.082057 (2020) doi:10.1101/2020.05.07.082057.

58. Hojman, P. *et al.* Fibroblast growth factor-21 is induced in human skeletal muscles by hyperinsulinemia. *Diabetes* **58**, 2797–2801 (2009).

59. Zheng, G. X. Y. *et al.* Massively parallel digital transcriptional profiling of single cells. *Nature Communications* **8**, 1–12 (2017).

60. Kang, H. M. *et al.* Multiplexed droplet single-cell RNA-sequencing using natural genetic variation. *Nature Biotechnology* **36**, 89–94 (2018).

61. Butler, A., Hoffman, P., Papalexi, E., Smibert, P. & Satija, R. Integrating single-cell transcriptomic data across different conditions, technologies, and species. *Nature Biotechnology* **36**, (2018).

62. Van Der Maaten, L. J. P. & Hinton, G. E. Visualizing high-dimensional data using t-sne. *Journal of Machine Learning Research* **9**, 2579–2605 (2008).

63. Qiu, X. *et al.* Reversed graph embedding resolves complex single-cell trajectories. *Nature Methods* **14**, 979–982 (2017).

64. Qiu, X. *et al.* Single-cell mRNA quantification and differential analysis with Census. *Nature Methods* **14**, 309–315 (2017).

65. la Manno, G. *et al.* RNA velocity of single cells. *Nature* **560**, 494–498 (2018).

66. Reimand, J. *et al.* g:Profiler-a web server for functional interpretation of gene lists (2016 update). *Nucleic acids research* **44**, W83–W89 (2016).

67. Supek, F., Bošnjak, M., Škunca, N. & Šmuc, T. Revigo summarizes and visualizes long lists of gene ontology terms. *PLoS ONE* **6**, (2011).

68. Walter, W., Sánchez-Cabo, F. & Ricote, M. GOplot: An R package for visually combining expression data with functional analysis. *Bioinformatics* **31**, 2912–2914 (2015).

69. Hu, H. *et al.* AnimalTFDB 3.0: a comprehensive resource for annotation and prediction of animal transcription factors. *Nucleic acids research* **47**, D33–D38 (2019).

70. Timshel, P. N. (in preparation). (2019).

71. Finucane, H. K. *et al.* Partitioning heritability by functional annotation using genome-wide association summary statistics. *Nature Genetics* **47**, 1228–1235 (2015).

72. Sun, W. *et al.* snRNA-seq reveals a subpopulation of adipocytes that regulates thermogenesis. *Nature* **587**, 98–102 (2020).

73. Stuart, T. *et al.* Comprehensive Integration of Single-Cell Data. *Cell* **177**, 1888-1902.e21 (2019).

74. Butler, A., Hoffman, P., Papalexi, E., Smibert, P. & Satija, R. Integrating single-cell transcriptomic data across different conditions, technologies, and species. *Nature Biotechnology* **36**, (2018).

Supporting Information

Supplementary Tables S1-S12 are not available with this version

Figures

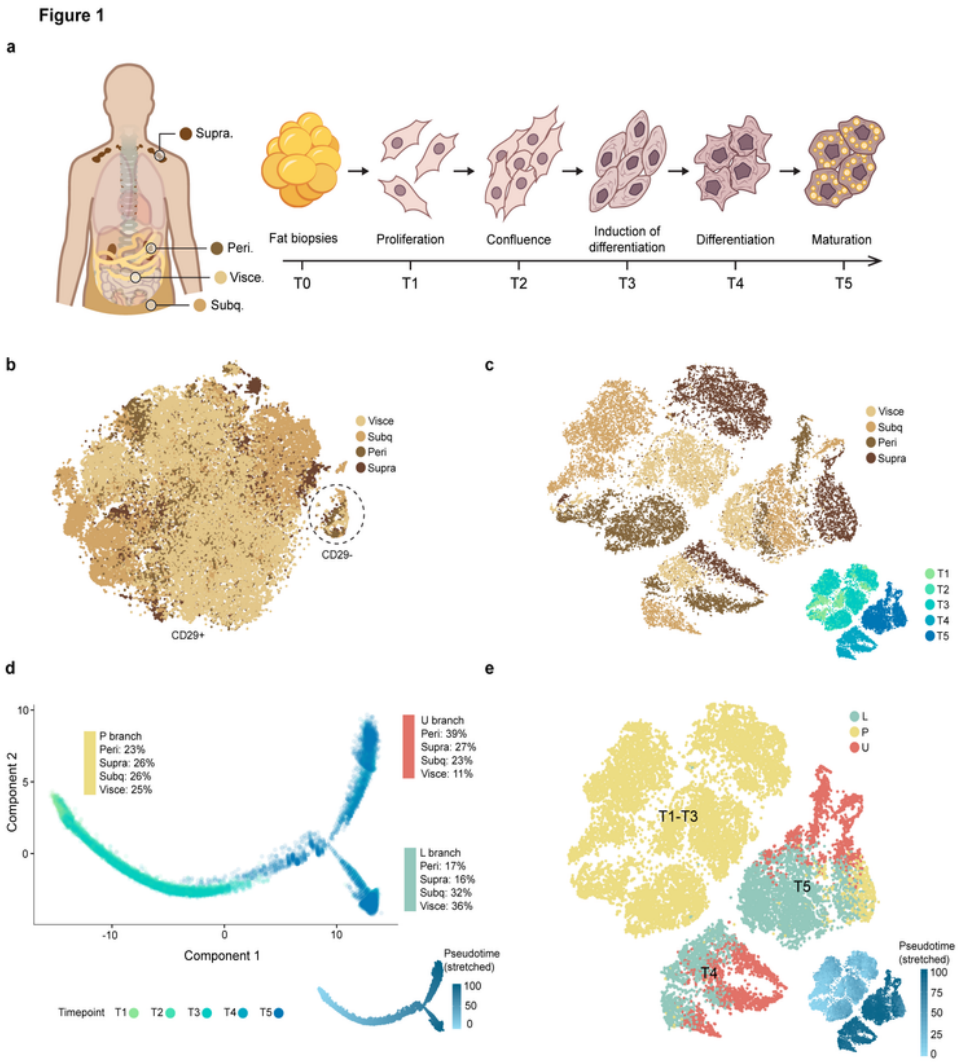

Figure 1

Single-cell trajectory analysis of developing adipocyte progenitors. Human adipocyte progenitors isolated from tissue biopsies of four adipose depots were harvested at five time points (T1-T5) during in vitro differentiation and subsequent single cell analysis was performed using the 10x genomics platform. **a)** Overview of adipose depots and cellular developmental stages. **b**) t-SNE atlas generated using the Seurat alignment algorithm[74], analyzing proliferating adipocyte progenitors (T1) derived from 11 individuals.

Peri (perirenal), Subq (subcutaneous), Supra (Supraclavicular), Visce (Visceral). **c**) t-SNE atlas of developing adipocyte progenitors (T1-T5) of four adipose depots from different individuals. The inset in the upper right corner indicates harvest time point. Clustering analysis grouped T1-T3 samples by adipose depot and T4 and T5 samples by time point and adipose depot. **d)** Monocle pseudotime trajectory of adipocyte progenitors from T1-T5. Cells from T1-T3 form a progenitor (P) branch that branches into two cell fates of the upper (U) and lower (L) branches containing cells after induction of differentiation (T4 and T5). Cells from all depots are represented in the U and L branches (the percentage of cells from each depot is indicated for each branch). The inset (lower right corner) shows the trajectory colored by stretched pseudotime that quantitatively measures how far a adipocyte progenitor has progressed through development. Stretched pseudotime is a normalized pseudotime scale ranging from 0 (least progressed) to 100 (most progressed). **e**) Cell atlas colored by trajectory branch identities. The bottom right inset shows the cellular development as measured by pseudotime.

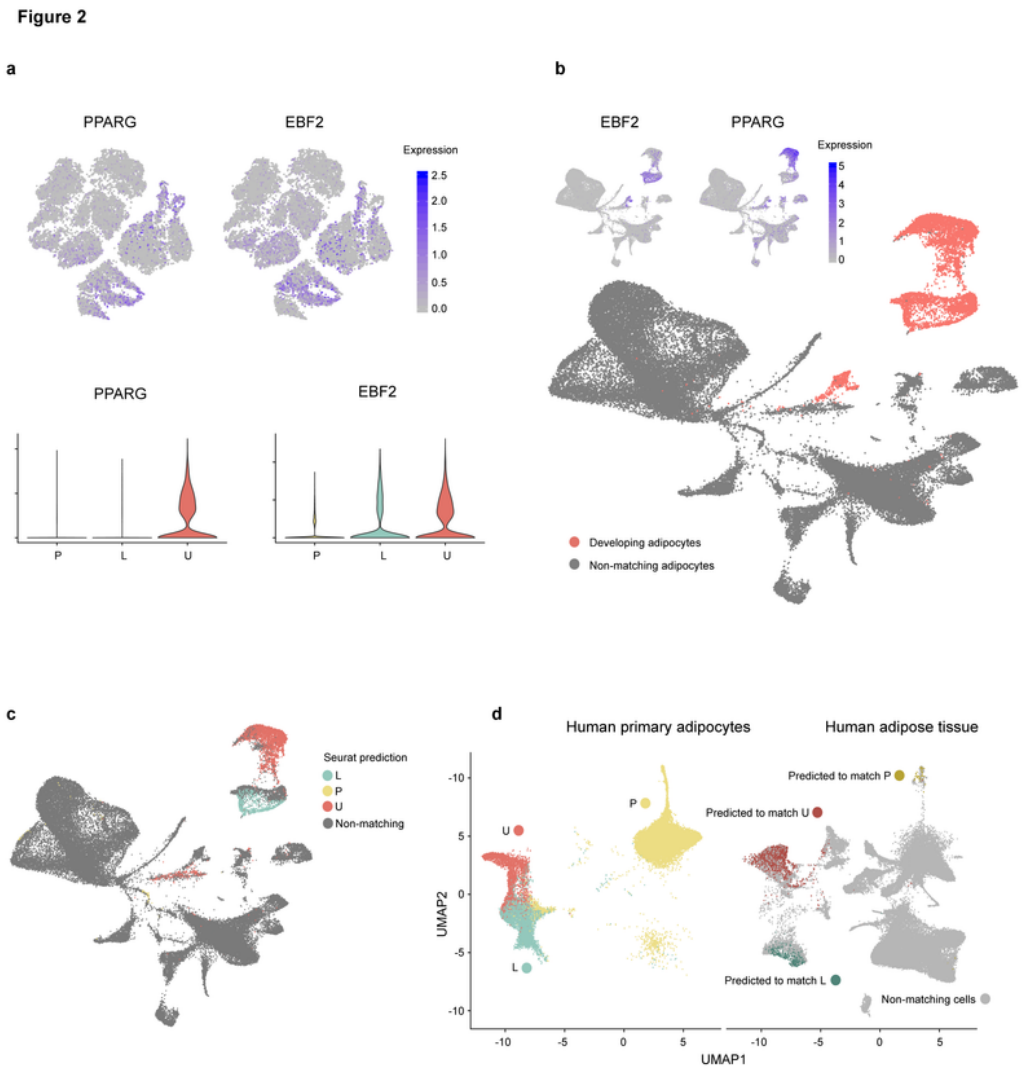

Figure 2

Comparing the single cell data set with human in vivo data. a) Feature plots highlighting the gene expression of adipogenic markers *EBF2* and *PPARG* in blue, demonstrating the temporal expression of these markers in our in vitro dataset. Violin plots in the bottom demonstrate branch-specific expression. **b)** Cell atlases of brown adipose tissue single-nuclei RNA sequencing from 16 humans (the *"BAT in vivo dataset")*[72] Selective expression of adipogenic markers *EBF2* and *PPARG* is highlighted in blue in the

feature plots on top. The sum of this expression was used to estimate an adipocyte population, highlighted in red in the cell atlas in the bottom. **c**) The in vitro adipocyte data set containing P, U and L branches was used as reference for Seurat data integration and label transfer to predict cell labels for the BAT in vivo dataset. Gray-colored cells did not match any of the cells in the developing adipocytes data. On top: Feature plots of main markers for the U (*APIPOQ*) and L (*DCN*) branches, respectively. **d)** Validation of Seurat data integration using Harmony. The figure shows cells projected in the integrated Harmony data embedding [30]. We used default parameters and recommended settings for the Harmony analysis.

Figure 3

Branch-specific differences metabolic and extracellular matrix signatures. a) BEAM analysis identified six kinetic clusters of branch-dependent genes. **b**) Expression dynamics are displayed as a function of pseudotime (stretched, ranging from 0 to 100) of marker genes for the U branch (*ADIPOQ, UCP2*) and the L branch (*DCN, APOD*). Solid lines show smoothed expression curves for each branch. **c)** FISH staining of human brown adipocytes harvested at T5 (halfway through full maturation) using RNA scope probes for branch marker genes. **d)** Top: Feature plots highlighting the gene expression of UCP1, UCP2 and UCP3 in blue. Bottom left: Predicted brown and white adipocyte content using BATLAS. Cells are grouped by each developmental branch and pseudotime decile. Bottom right: FISH staining using RNA scope probe targeting UCP2 combined with antibody staining targeting mtHSP70. **e)** GO term enrichment analysis visualized using REViGO and the GOplot R package.

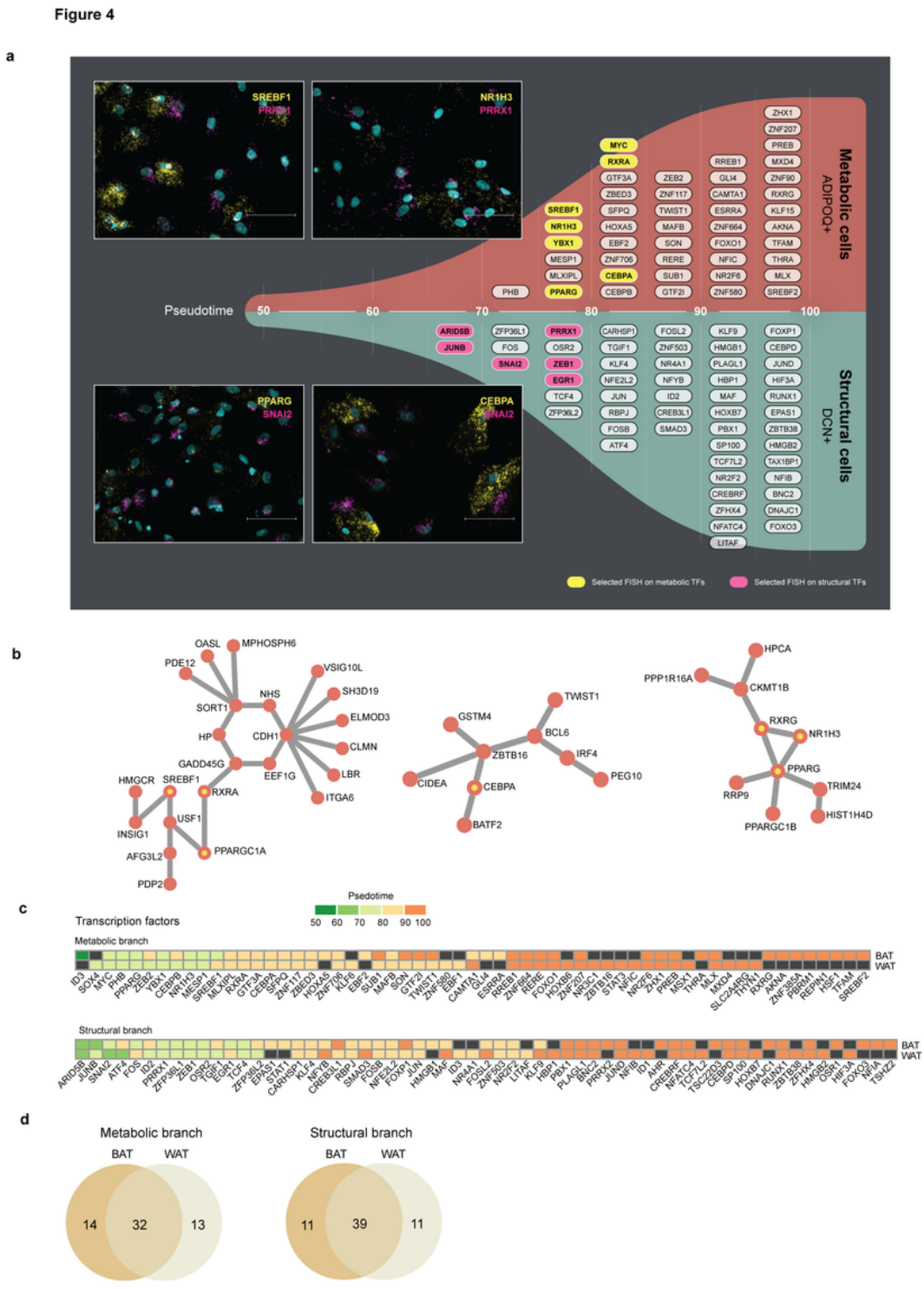

Figure 4

Branch-specific expression of Transcription Factors. a) Transcription factors identified as increasing in expression in one branch over another are indicated on respective branches, at the stretched pseudotime point where the smoothed gene expression is observed to diverge. Inset images are from RNA-FISH labeling in brown adipocytes of select combinations of transcription factors from the two branches, showing the distinct labeling of branch-specific transcription factors. **b)** Scellnetor analysis identified key

transcriptional networks enriched in the metabolic branch, confirming the role of several transcription factors identified above as involved in metabolic cell type development. **c)** Branch-specific transcription factor analysis performed independently for brown (perirenal + supraclavicular) and white (visceral + subcutaneous) depots. Color scale indicates pseudotime point at which expression of a gene diverges between branches, and a black box indicates that there is no divergence in gene expression between branches. A shared set of transcription factors characterize early differentiation across depots whereas further differentiation proceeds through depot-specific TF. **d)** Venn diagrams indicating the extent of common and distinct transcription factors involved in the development of each branch in brown and white adipocyte differentiation.

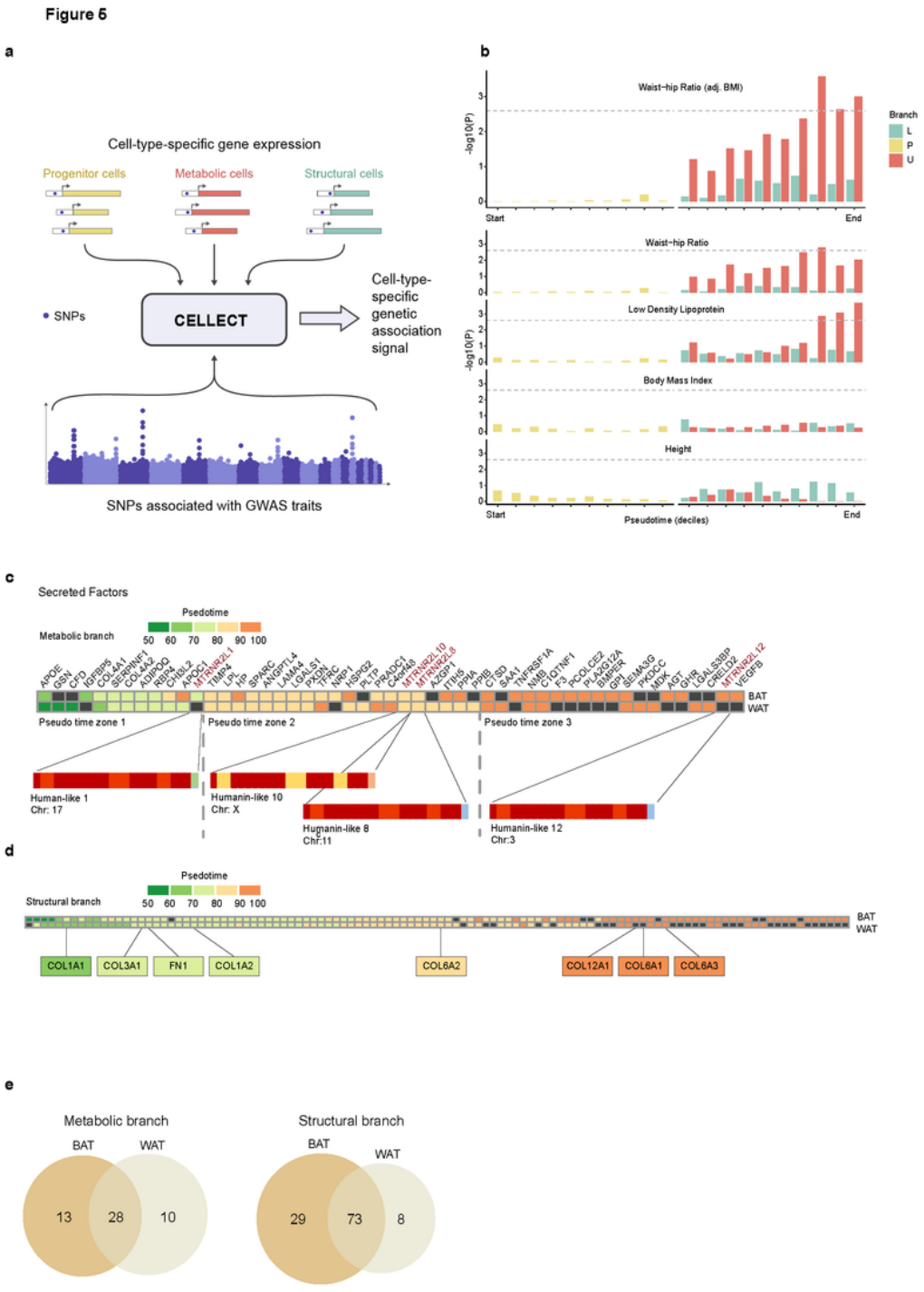

Figure 5

Metabolic characterization of the metabolic and structural branches. a) CELLECT[45] cartoon **b)** CELLECT analysis of progenitor, upper (metabolic), and lower (structural) branch cells, binned by pseudotime deciles. Metabolic cells with highest pseudotime values show significant association with WHR (adjusted to BMI) and LDL. Other traits did not reveal any significant association. **c)** Metabolic branch-specific expression patterns of predicted secreted proteins, separated by origin from brown

(supraclavicular+perirenal) and white (subcutaneous+visceral) depots. Several Humanin-like peptides with cytoprotective effect are expressed in the metabolic branch, with a higher number of these peptides expressed specifically in brown adipocytes. A black box indicates that there is no divergence in gene expression between branches **d)** The structural branch is characterized by branch-specific expression of ECM components. A black box indicates that there is no divergence in gene expression between branches. **e)** Venn diagram demonstrating number of genes predicted to encode secreted proteins dependent on branch and BAT or WAT origin.

Supplementary Files

This is a list of supplementary files associated with this preprint. Click to download.

- Extendedfigurelegends.pdf
- FigureS1.pdf
- FigureS2.pdf
- FigureS3.pdf
- FigureS4.pdf
- FigureS5.pdf
- FigureS6.pdf
- FigureS7.pdf
- FigureS8.pdf
- FigureS9.pdf